

U(PM)²: Unsupervised polygon matching with pre-trained models for challenging stereo images

Chang Li[†] Xingtao Peng

Key Laboratory for Geographical Process Analysis & Simulation of Hubei Province
Central China Normal University

lcshaka@126.com

lichang@ccnu.edu.cn

pengxt@mails.ccnu.edu.cn

Abstract

Stereo image matching is a fundamental task in computer vision, photogrammetry and remote sensing, but there is an almost unexplored field, i.e., polygon matching, which faces the following challenges: disparity discontinuity, scale variation, training requirement, and generalization. To address the above-mentioned issues, this paper proposes a novel U(PM)²: low-cost unsupervised polygon matching with pre-trained models by uniting automatically learned and handcrafted features, of which pipeline is as follows: firstly, the detector leverages the pre-trained segment anything model to obtain masks; then, the vectorizer converts the masks to polygons and graphic structure; secondly, the global matcher addresses challenges from global viewpoint changes and scale variation based on bidirectional-pyramid strategy with pre-trained LoFTR; finally, the local matcher further overcomes local disparity discontinuity and topology inconsistency of polygon matching by local-joint geometry and multi-feature matching strategy with Hungarian algorithm. We benchmark our U(PM)² on the ScanNet and SceneFlow datasets using our proposed new metric, which achieved state-of-the-art accuracy at a competitive speed and satisfactory generalization performance at low cost without any training requirement.

1. Introduction

Stereo image matching is establishing correspondences between images captured from different viewpoints [17], and achieving high accuracy and robust correspondences in this process is vital for a wide range of downstream tasks. Currently, handcrafted feature-based and deep-learning-based methods have achieved remarkable progress in point or line correspondence as below: 1) Point matching aims to find corresponding individual points between images. Classic algorithms such as SIFT [9] have been augmented and often surpassed by deep learning-based methods such as SuperPoint



Figure 1. A visual representation of the different types of matching primitives (points, lines, polygons).

[3] and LoFTR [15] that learn features directly from data, achieving superior matching accuracy and robustness. 2) Line matching [8] focuses on establishing correspondences between line segments and provides structural information; 3) Hybrid point-line matching, GlueStick [13] unified point and line into a single wireframe structure to achieve more accurate and reliable point-line matching results. However, there are still no reports on higher-level structural feature matching such as polygon matching, especially direct matching of vector contours from stereo images. Some recent methods used for other tasks are considered to be similar to polygon matching in visualization. MESA [18] leverages homogeneous areas to refine point matching; and MASA [7] track and match the same areas also obtained by segment anything model (SAM) [5] from different video frames. Therefore, as shown in Fig. 1, this paper extends the concept

[†]Corresponding authors: Chang Li

of image matching (i.e., point and line) to a higher dimension: polygon matching (i.e., face), which possesses a clear geometric structure and semantic meaning.

Polygon offers a more comprehensive representation of scene structure than individual point and line, so it is particularly crucial in scenarios demanding high-level scene understanding, such as urban reconstruction from aerial imagery or detailed 3D modeling for augmented reality. Polygon matching has not been explored yet, and faces some key challenges: 1) large-format imagery matching, demands robust solutions to large-scale variation for remote sensing imagery, which includes adapting to both the sheer size of the images and the significant scale differences between corresponding polygons across stereo pairs; 2) local disparity discontinuities (Fig. 2), leads to local topological inconsistencies, so related algorithm should be designed to overcome this contradiction; 3) generalization, should be ensured in unsupervised (i.e., training-free) polygon matching under low computational power.

To address the aforementioned challenges in stereo polygon matching, we propose a novel low-cost unsupervised polygon matching with pre-trained models $U(PM)^2$. $U(PM)^2$ aims to establish fine-grained polygon-to-polygon correspondences in stereo images through a multi-stage pipeline designed to tackle scale variation, search efficiency, local disparity discontinuities and generalization with training-free strategy, including the following: Firstly, the feature points and vector polygons are detected in images by the detector with pre-trained models, laying the foundation for subsequent matching. Secondly, to address the challenge of scale variation inherent in large-format images, the global matcher leverages the bidirectional-pyramid matching strategy to generate the adaptive search window, which progressively narrows the search space in the image pyramid, significantly reducing computational cost while maintaining matching accuracy. Finally, we refine the matching results by local-joint geometry and multi-feature matching strategy (LoJoGM) with the Hungarian algorithm. This step is crucial for mitigating local disparity discontinuities, as it considers the local relationships between polygons and polygons from stereo images, and addresses topological inconsistencies in the target as the viewpoint changes. By integrating automatically learned features with handcrafted features with optimized matching strategy, $U(PM)^2$ offers a low-cost and generalized solution for stereo polygon matching without any training requirement.

In summary, this paper makes the following key contributions to the field of stereo image matching: **1)** We propose a novel low-cost unsupervised polygon matching framework $U(PM)^2$ that effectively integrates automatically learned features from pre-trained models with handcrafted geometric constraints. Moreover, in our framework, any module (eg., pre-trained model) can be replaced by more advanced algo-

rithms. This work advances the field of feature matching, upgrading from 0/1D (point/line) primitives, thus providing a comprehensive solution for correspondence problems. **2)** We propose a global matcher based on a bidirectional pyramid strategy with pre-trained LoFTR, which addresses the critical challenge of scale variation in large-format imagery, enabling efficient and accurate polygon matching in challenging scenarios. **3)** A local-joint geometry and multi-feature matching strategy, i.e., LoJoGM is proposed that effectively mitigates local disparity discontinuities by considering both graph and texture features, along with multi-geometric constraints and Hungary matching, resulting in more robust and consistent matching results. **4)** We establish a novel evaluation metric specifically designed for polygon matching tasks and demonstrate the state-of-the-art (SOTA) performance of U(PM)² against existing methods using this metric as well as other commonly employed matching evaluation metrics.

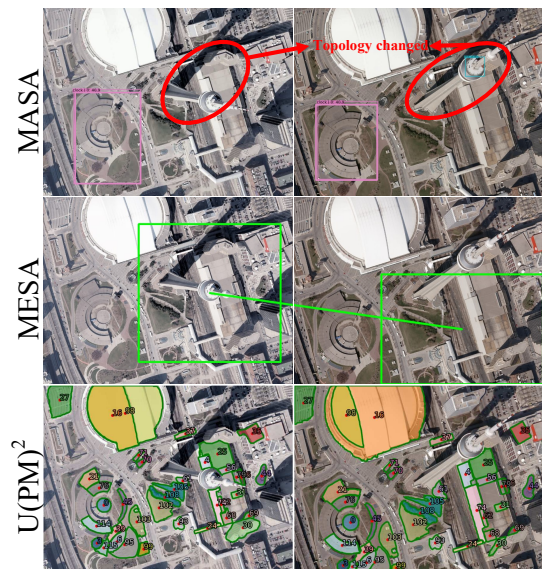


Figure 2. **U(PM)² vs. MASA and MESA in visual comparison.** The locations indicated by the rounded boxes are where the topological relationships have changed. MASA fails to detect polygons or areas because it was designed for different tasks. MESA achieves lower area overlap ratios and higher mismatch rates. In contrast, U(PM)² attains the highest number of matches with the finest-grained accuracy (down to individual building-level accuracy).

2. Related Work

2.1. Stereo matching

Stereo matching can be broadly classified into area-based matching (ABM) and feature-based matching (FBM). ABM approaches minimize a matching cost function to reduce mismatches or aggregate matching costs within local pixels

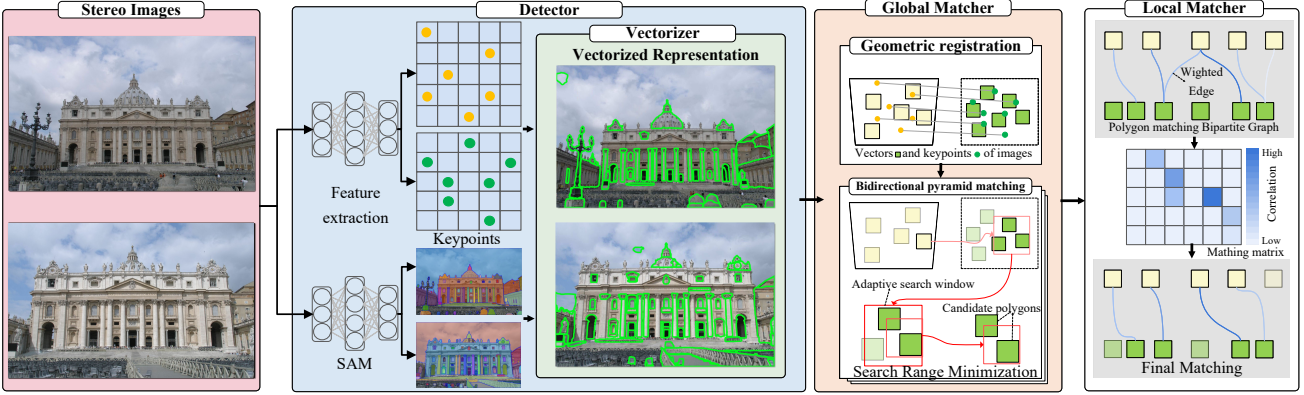


Figure 3. **Overview of U(PM)².** 1) Detector jointly performs polygon and feature point detection from stereo images to construct polygons with graphic structure. 2) Global matcher matches feature points extracted by the Detector, establishing reliable correspondences and global geometric constraints. 3) Local matcher eliminates ambiguous matches through the geometry and multi-feature matching strategy to solve bipartite graph matching, ultimately optimizing polygon matching.

as the matching criterion [10]. Traditional FBM approaches match images by extracting and computing feature descriptors. Deep learning-based FBM [6, 16] further advances this field by training neural networks to automatically learn feature representations. It enables obtaining precise matching in complex scenes, low-texture regions, and under occlusions. Both ABM and FBM are suitable for feature-rich scenes with large illumination variations but FBM has higher computationally efficient than ABM.

In contrast to these methods, we utilize a combination of ABM and FBM to obtain accurate polygon matching. The proposed U(PM)² utilizes both FBM to construct stable multi-view geometric constraints and ABM to quickly handle local image matching.

2.2. Polygon matching

Polygon matching for stereo images fundamentally differs from existing shape matching or geometric shape retrieval [4]. Instance segmentation-based object tracking methods, such as MASA [7], and area-to-area polygon matching methods, like MESA [18] and SGAM [19], represent related approaches. However, as shown in Fig. 2, both exhibit significant limitations. Specifically, MASA is suitable for target tracking tasks but not for polygon matching, particularly in complex real-world scenes. MESA exhibits lower area overlap ratios and higher mismatch rates, often failing to achieve building-level accuracy, and performs poorly under significant viewpoint changes. These limitations stem from: 1) MASA relies on the generalization of its object detection and tracking modules, suffering from mismatches on untrained targets (e.g., aerial imagery); 2) MESA and SGAM are designed for point matching rather than polygons and depend on robust spatial (i.e., graphic) relationships. However, disparity abrupt changes induce spatial inconsistencies,

leading to matching failures; and 3) the inherent sensitivity of both methods to large viewpoint variations.

In contrast, our proposed U(PM)² paradigm overcomes these drawbacks by: 1) targeting irregularly shaped segments with finer granularity, enhancing robustness to disparity discontinuities and scale variations; 2) directly producing vector outputs, enabling precise polygon matching; and 3) effectively handling stereo images with larger viewpoint variations without requiring any training.

3. Methodology

Fig. 3 shows an overview of the U(PM)², of which the modules are as follows.

3.1. Detector

The detector includes polygon detection and feature point detection. Polygon detection consists of the segmentor and the vectorizer: a pre-trained SAM is first used to perform zero-shot instance segmentation, producing object-level masks and bounding boxes; then, a vectorization step converts each mask contour into a polygonal representation. Next, the Douglas–Peucker algorithm is applied to simplify the vector nodes and remove edge noise due to raster–vector conversion. Finally, the graph G is constructed based on the nodes of the polygon:

$$G = (V, E), \quad (1)$$

where V represents the set of all vertices (i.e., the set of polygon vertices), and E denotes the set of undirected edges v_i , corresponding to the polygon edges. For point detection, U(PM)² integrates both handcrafted features (e.g., SIFT) and learned features (e.g., SuperPoint, LoFTR, LightGlue) to improve robustness and enable unsupervised polygon matching.

3.2. Global matcher

The global matcher contains the following key modules: 1) The initial matching module establishes fundamental correspondences between stereo image pairs by estimating a global homography matrix through a pre-trained LoFTR or others. 2) The bidirectional pyramid matching module dynamically optimizes search ranges across multi-scale pyramid features to balance computational efficiency and matching completeness. 3) Geometric rectification compensates distortions between polygon regions.

Initial matching. First, we use a feature matcher to get initial matching on the feature points extracted by the detector. This results in the fundamental matrix \mathbf{F} and the homography matrix \mathbf{H} which filler the mismatches by MAGSAC++[1], providing an approximate spatial correspondence for source polygons. Due to the significant viewpoint changes in stereo images, homography estimation is not always accurate. Therefore, before calculating the homography matches for the computed matched points, we first estimate the fundamental matrix, compute the epipolar lines, and then further filter out the matched feature points near these lines. It is important to note that the discarded feature points are still retained but excluded from the homography calculation. This method allows us to preserve many feature points for further matching in the subsequent steps.

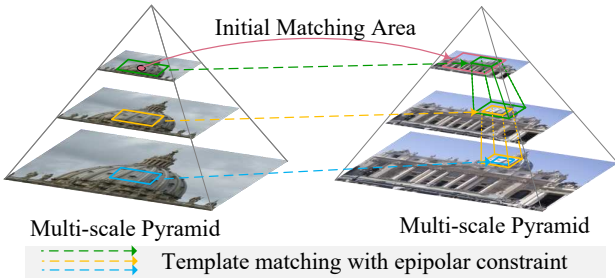


Figure 4. **Bidirectional-pyramid matching.** The Bidirectional pyramid progressively narrows the search region from the top-level initial area toward lower levels to establish geometric constraints for subsequent local matching.

Bidirectional-pyramid matching. To address the adaptation of the search range for matching images of varying sizes and to improve matching efficiency and accuracy, bidirectional pyramid matching is proposed. Fig. 4 shows that this strategy reduces computational complexity by combining multi-stage downsampling and adaptive search window and improves the matching accuracy by utilizing epipolar line constraints and template matching.

First, image Gaussian pyramids are created for the stereo images with a downsampling factor of 1/3. Stop sampling until the length or width of the image at the bottom of the Gaussian image pyramid is no higher than 200 pixels. For an image size of $W \times H$, n layers of pyramids, $\min\{W/3^n, H/3^n\} < 200$, so the time complexity of subsequent matching on large-format images is reduced. At the top level of the pyramid, the center c_i of the source polygon is transformed to c'_i in the target image using the homography matrix. A square window W_τ of size τ is then centered at c'_i , and a smaller window W_ϕ of size ϕ is centered at c_i .

Next, W_ϕ is used as a template to perform template matching with W_τ , identifying the most similar region W'_ϕ centered at c''_i in the target image:

$$W'_\phi = \left\{ (x, y) \mid |x - x_{c''_i}| \leq \frac{\phi}{2}, |y - y_{c''_i}| \leq \frac{\phi}{2} \right\}, \quad (2)$$

where x, y denote the coordinates of points. Subsequently, The candidate matching region W'_ϕ is then filtered using epipolar constraints. The epipolar constraint is used to evaluate whether the center points c''_i of the matching region are within a range ϵ above or below the epipolar line based on the fundamental matrix \mathbf{F} :

$$|\mathbf{p}_{\text{right}}^\top \mathbf{F} \mathbf{p}_{\text{left}}| \leq \epsilon, \quad (3)$$

where, the point c and c''_i are first homogenized into $\mathbf{p}_{\text{left}} = (x_c, y_c, 1)^\top$ and $\mathbf{p}_{\text{right}} = (x_{c''_i}, y_{c''_i}, 1)^\top$.

Finally, W'_ϕ is projected onto the lower levels of the pyramid, and the process is repeated. Typically, passing through four pyramid levels is sufficient to narrow down the search to an accurate range W_{final} . The target polygons within the W_{final} are considered the candidate matching polygon for the corresponding source polygon. This process is repeated for all source polygons $\mathcal{A} = \{G_i\}_{i=1}^m$ and target polygons $\mathcal{B} = \{G'_j\}_{j=1}^n$ to obtain the coarse matching result $\mathbf{M} \in \{0, 1\}^{m \times n}$. m and n represent the number of source polygons and target polygons, respectively. $\mathbf{M}_{ij} = 1$ when G_i matches G'_j . \mathcal{A} and \mathcal{B} are many-to-many relationships, and further refinement of the matching is required in the Local Matcher to optimize the matches to one-to-one relationships and to eliminate some false matches.

Deep-Spectral factor. Geometric distortions are present in homonymous polygons in stereo images due to segmentation results, viewpoint differences, and scale transformations. To overcome the geometric distortion, geometric correction is required using homonymous points matched by LoFTR within the range of the source and target polygons. Specifically, for any candidate match $\mathbf{M}_{ij} = 1$ in $\mathbf{M} \in \{0, 1\}^{m \times n}$, we identify the pairs of homonymous keypoint matches M_{kp} in the stereo image. Then, count the number of matching

pairs m_{kp} as the deep-spectral factor χ that located within G_i and G_j :

$$\chi = |\{m_{kp} | m_{kp} \in M_{kp}\}|. \quad (4)$$

The count of matched feature points serves as a crucial basis for the subsequent local matching process. Specifically, When χ satisfies the condition for computing homography, the homography matrix \mathbf{H}' can be computed within the polygon. The homographic relationship of the local image can be computed based on the corresponding points located within G_i and G_j , respectively. Then, G_i and G_j are registered, which helps reduce their geometric distortion. This enables the further calculation of geometric correlation.

Please note that global matcher failure may occur due to local disparity inconsistency or texture similarity.

3.3. Local matcher

To solve the aforementioned problem, the local matcher is proposed to optimize the matching (Fig. 5). 1) Local geometric correlation is computed between source and candidate polygons. 2) When geometric constraints are insufficient, as indicated by a low deep-spectral factor, it adapts to texture similarity correlation. Regardless of the correlation type, a matching score is generated and converted into a cost function. 3) The LoJoGM minimizes the total cost to determine optimal polygon correspondences, ensuring robust matching even with limited geometric constraints.

Local geometric correlation. In local matching, local geometric distortions pose a significant obstacle to accurate polygon matching. Even though preliminary registration may have been performed in the global matching, geometric distortions still exist locally due to the registration errors being globally optimal. To address this issue, we propose local geometric correlation, which is designed to further reduce local geometric distortions or ambiguities in the polygons to be matched. First, If the deep-spectral factor satisfies the conditions for a local homography transformation, the polygon is corrected locally. Then, the local geometric correlation is described by both their area discrepancy and geometric discrepancy. For the local geometric discrepancy β , we compute it using the graph-matching algorithm [4]. It represents each node v_i in all N nodes of the graph (i.e., polygons) using its top- k neighboring nodes embedding α_i . This enables the conversion of the graph into a vector embedding $\mathbf{A} = (\alpha_1, \dots, \alpha_N)^\top$.

$$\alpha_i = (e_1^i, e_2^i, \dots, e_k^i), \text{ where } 1 \leq k \leq N-1, \quad (5)$$

$$e_k^i = \frac{d(v_i, v_{\mathbb{E}(v_i, k)})}{\sum_{l=i}^{\mathbb{E}(v_i, k)-1} d(v_l, v_{l+1})} \sum_{l=i}^{\mathbb{E}(v_i, k)-2} v_l \widehat{v_{l+1} v_{l+2}}, \quad (6)$$

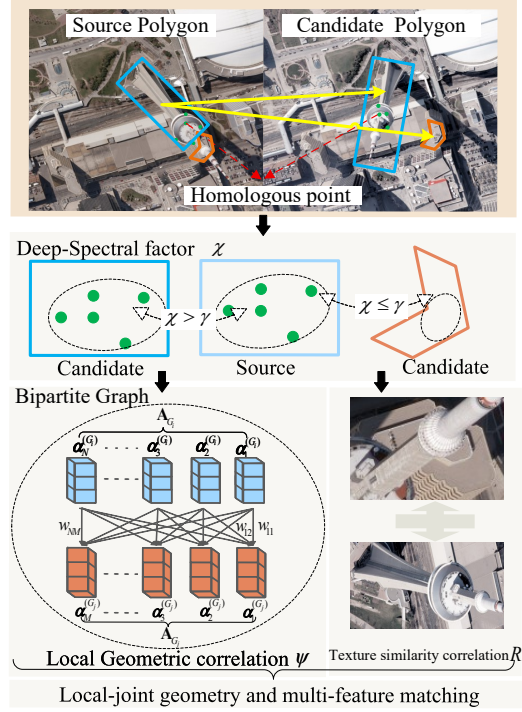


Figure 5. The proposed Local Matcher. It addresses matching failures caused by local deformations and topological inconsistencies. The essential reason is the viewpoint variation causes disparity variation, then disparity variation in turn leads to topological inconsistency (e.g., the relative position relationship between the box and the polygonal area). To solve above-mentioned issue, the local matching is proposed by joint local geometric and texture correlations.

where $d(u, v)$ is the Euclidean distance between nodes u and v , and the $v_l \widehat{v_{l+1} v_{l+2}}$ is the angle between v_l , v_{l+1} and v_{l+2} . The function $\mathbb{E}(v_i, k)$ denotes index m such that node v_m is the k -th nearest neighbor of v_i in Euclidean space. To compare the difference between two graphs, a complete bipartite graph \mathcal{G}_{ij} with two node sets $u_i \in G_i$ and $v_j \in G_j$ is constructed. The weight w_{ij} of each edge in the graph is the Euclidean distance between the node vectors \mathbf{A}_{G_i} and \mathbf{A}_{G_j} . Next, the Hungarian algorithm is applied to \mathcal{G}_{ij} to obtain the minimum weighted matching cost, which serves as the geometric discrepancy β and the nodes matching matrices \mathbf{M}_{node} between G_i and G_j :

$$\beta = \min \|\mathbf{M}_{\text{node}}\|_2. \quad (7)$$

Finally, we use both the area discrepancy η and the geometric shape difference β to jointly describe the local geometric correlation ψ_{ij} between G_i and G_j :

$$\psi_{ij} = \xi \cdot \left(1 - \left| \frac{\eta_i - \eta_j}{\max(\eta_i, \eta_j)} \right| \right) + \exp(-k \cdot \beta). \quad (8)$$

Here, ξ denotes the weight ratio between the impact of area and shape differences on local geometric similarity, while k is a scaling factor for shape differences, adjusted to align the scale of both types of differences. η_i and η_j represent the area of the G_i and G_j , respectively.

Texture similarity correlation. Under the condition that the deep-spectral factor does not satisfy the local correction, then the texture features are computed directly. For texture features, to be able to effectively deal with images with large radiometric differences, we use normalized correlation coefficient templates to match similar texture features, as it has radiometric linear invariance and can cope with images with large radiometric differences. We compute the correlation coefficient R between the image patch I and target patch T within the bounds of the source and candidate polygon. Finally, we combine local geometric correlation ψ and texture similarity correlation R to calculate the matching cost ζ between the source polygon and candidate polygons:

$$\zeta = \begin{cases} \frac{1}{\psi + 10^{-5}} & \text{If } \chi > \gamma \\ \frac{1}{\max(0.5, R) + 10^{-5}} & \text{else} \end{cases}. \quad (9)$$

Here, γ represents the threshold about χ that is considered under varying conditions of deep-spectral factor. In regions with fewer corresponding points, texture features can still be leveraged to increase the number of matches. Our experiments later demonstrate that jointly considering geometric and texture features effectively improves both matching accuracy and match quantity.

Local-joint geometry and multi-feature matching. Local-joint geometry and multi-feature matching strategy (LoJoGM) is proposed to solve issue of local topological inconsistencies and abrupt disparity changes in Fig. 2 and Fig. 5. Unlike methods that solely prioritize only one to many local overall minimization, our LoJoGM leveraging Hungarian algorithm performs many-to-many optimization, i.e., the target and neighboring polygons (many) to achieve optimal and reliable matching with candidate region polygons (many). It effectively mitigates the impact of topological inconsistencies and disparity mutations, and improves the matching reliability by confining them to a consistent spatial context because it does not rely on global spatial relationships. The proposed LoJoGM provides a robust solution to the challenges caused by local disparities and topological variations.

Specifically, we convert the multi-matching relationship between source $\mathcal{A} = \{G_i\}_{i=1}^m$ and target polygons $\mathcal{B} = \{G'_j\}_{j=1}^n$ into a bipartite graph $\mathcal{M} = (\mathcal{A}, \mathcal{B}, \mathbf{E}, \zeta)$, where edges $\mathbf{E}_{ij} = (G_i, G'_j) \in \mathbf{E}$ in the bipartite graph are weighted by the matching cost $w(\mathbf{E}_{ij}) = \zeta_{ij}$. Finally, the optimal local match \mathcal{M}' is found by minimizing the global cost $w(\mathcal{M}')$ using the position-independent Hungarian al-

gorithm, which considers only weights.

$$w(\mathcal{M}') = \sum_{n=0}^{|M'|} \zeta_{\mathbf{E}'_n}, \mathbf{E}'_n \in \mathcal{M}'. \quad (10)$$

Finally, $\{E'_n\}_{n=0}^{|M'|}$ is an overall accurate polygonal matching of the two stereo images is obtained.

3.4. Metric for polygon matching

Unlike point-line matching accuracy evaluation, polygon matching tasks needs to consider discrete metrics(i.e., precision and recall) rather than global errors due to geometric properties. And the discrete metrics are evaluated by the ground truth (GT) of polygon matching, so we design the scheme to generate the GT of polygon matching. We project the geometric center $\mathbf{x}_i = (p, q, 1)^\top$ of polygon G_i to \mathbf{x}'_i in G_j onto the target image:

$$x'_i = \mathbf{P}_1 \cdot \left(\mathbf{T}_R^{-1} \cdot \mathbf{T}_L \cdot d \cdot [\mathbf{P}_0^{-1} x_i \quad 1]^\top \right)_{\text{proj}}. \quad (11)$$

Here, \mathbf{P}_0 and \mathbf{P}_1 are the intrinsic matrices of the right camera. \mathbf{T}_R and \mathbf{T}_L are the transformation matrices of the right and left cameras, respectively. d denotes the depth value of the image. The projection operator \cdot_{proj} converts normalized coordinates to pixel coordinates by dividing them by depth dimension. Then, we leverage a bidirectional consistency check to refine the GT of matching relationships M_{ij} :

$$M_{ij} = \mathbb{I}(\|x_i - x'_i\|_2 \leq \lambda). \quad (12)$$

Here, the indicator function $\mathbb{I}(\cdot)$ returns 1 if the specified condition is satisfied and 0 otherwise. Parameters λ empirically threshold. Discrete metrics in polygon matching can be evaluated through the GT of homologous image points and the geometric properties of polygons, which are often unmeasurable in point or line matching tasks.

4. Experiments

4.1. Experimental setup

U(PM)² conducted performance evaluations on SceneFlow [11], KITTI (IN APPENDIX) [12], ScanNet [2] and IS-PRS [14] (large-format images) running on L40 (48GB). We combined LoFTR, Superpoint, and Lightglue with U(PM)² and compared with recent related methods. The pyramid downsampling factor is set to 3, with the width or height of the top-level image limited to 200 pixels. The search window size for the source polygon is 15x15, and the initial search range for the target polygon is 50x50. We employ Symmetric Area Score (SAS) for matching completeness, Matching Precision (MP) under three thresholds (80/50/40, %), and precision as discrete metrics. Details are presented in APPENDIX.

Dataset	Method	Matching Precision (%) \uparrow			Symmetric Area Score (%) \uparrow			Matches \uparrow	Time(s) \downarrow
		MP ₄₀	MP ₅₀	MP ₈₀	SAS ₄₀	SAS ₅₀	SAS ₈₀		
SceneFlow	MESA CVPR'24	36.23	36.20	35.96	4.45	4.45	4.46	12.05	47.52
	SGAM arXiv'24	40.31	40.29	40.13	4.37	4.46	4.46	16.00	11.08
	MASA CVPR'24	29.19	30.37	30.06	13.31	13.31	13.31	3.04	2.18
	U(PM) ² +Superpoint+LightGlue	68.60	68.57	68.51	25.51	25.60	25.68	27.50	3.27
	U(PM) ² +LoFTR	44.95	44.91	44.74	29.66	29.68	29.70	20.59	16.94
ScanNet	MESA CVPR'24	13.52	13.50	13.63	11.84	11.85	11.85	6.22	25.41
	SGAM arXiv'24	16.94	16.92	17.00	21.07	21.07	21.08	11.23	7.08
	MASA CVPR'24	14.50	14.13	14.66	12.13	12.13	12.13	2.03	1.20
	U(PM) ² +Superpoint+LightGlue	17.39	17.41	17.59	15.94	15.94	15.94	5.01	2.48
	U(PM) ² +LoFTR	21.25	21.50	21.05	17.12	17.08	17.66	6.32	1.42

Extended Data Table 1. **Evaluation on SceneFlow and ScanNet datasets for metrics of polygon matching.**

4.2. Polygon Matching

As shown in the Table 1, we present a comprehensive evaluation of our U(PM)² against several similar methods on the SceneFlow and ScanNet datasets. Our U(PM)² combined with SuperPoint and LightGlue reached 68.60% in MP, which is a substantial improvement at the second-fastest speed over competing methods like MESA (36.23%), SGAM (40.31%) and MASA (29.19%). While the combination with LoFTR also shows strong results, the SuperPoint and LightGlue pairing demonstrates a superior balance of high precision and completeness, with a remarkable increase in the number of correct matches.

Table 2 shows the sensitivity of the method to different geometric similarity thresholds. Higher weight indicates that area has a greater influence on geometric similarity, but since U(PM)² has aligned the polygons to the same scale during matching, the area difference between matched pairs is small. Finally, an optimal matching accuracy of 87.50% was achieved on the sceneflow dataset.

See the appendix for further quantitative/qualitative experiments and an analysis of pre-trained model size. These results demonstrate U(PM)² achieves SOTA performance on both synthetic and real-world benchmarks. It outperforms the next-best method by 28.29% in MP at the second-fastest speed, and improving the quantity and quality of polygon matches.

Method	Recall(%) \uparrow	Precision(%) \uparrow	F1 \uparrow
U(PM) ² @5	72.17	87.04	0.79
U(PM) ² @6	72.67	87.50	0.79
U(PM) ² @7	72.72	87.44	0.79

Extended Data Table 2. **Evaluating on SceneFlow dataset.**

Method	Resolution	Time(s) \downarrow	ACR(%) \uparrow	Num \uparrow
U(PM) ² (Full)	5750 \times 3750	10.49	21.92	17.10
U(PM) ² ($\mathcal{L} = 2$)	5750 \times 3750	10.70	21.92	17.10
baseline	5750 \times 3750	15.66	21.92	17.10
U(PM) ² (Full)	11500 \times 7500	18.95	23.15	10.7
U(PM) ² ($\mathcal{L} = 2$)	11500 \times 7500	18.96	23.15	10.7
baseline	11500 \times 7500	24.86	23.15	10.7

Extended Data Table 3. **Evaluation of U(PM)² on ISPRS dataset under different pyramid levels.** U(PM)² (Full) denotes the levels ensuring the top-layer resolution of the constructed image pyramid does not exceed 200 pixels. The baseline uses a fixed range instead of the bidirectional pyramid.

4.3. Matching in challenging imagery

To validate the scalability and efficiency of our proposed U(PM)² framework in challenging imagery, we conducted experiments on large-format stereo-image pairs. ISPRS remote dataset [14] presents significant challenges due to its high resolution between images. Specifically, we assessed the impact of our bidirectional pyramid matching strategy on both matching accuracy and computational efficiency. We hypothesized that the pyramid approach would significantly reduce computational efficiency (Time) while maintaining acceptable Area Coverage Ratio (ACR). Table 3 presents the quantitative results of our experiments, showcasing the effectiveness of U(PM)² in handling large-format images.

4.4. Ablation Study

To evaluate the effectiveness of each module in U(PM)², we conducted a comprehensive ablation study (Table 4). After removing pyramid matching and LoJoGM, we observed significant decreases in all metrics, particularly after removing LoJoGM. The results demonstrate these modules are

indispensable for the polygon matching task.

Pyramid matching. The goal of pyramid matching is to provide an adaptive search window. For the ablation of the pyramid matching, we employed a standard approach to define the search window. Specifically, for each source polygon G_i in the left image of the stereo pair, a search range R_i is defined in the right image with a radius corresponding to the shortest side of the bounding box B_i around G_i . During global matching, candidate polygons are searched within the range R_i . Most polygons have smaller search ranges R_i , so fewer polygons need to be matched during the subsequent local matching stage, leading to faster processing. However, this also results in fewer final matches. Moreover, for more challenging tasks, such as matching small targets in large-scale images, the static nature of R_i can lead to more misses due to its smaller scale compared to the overall image size.

Method	ACR(%) \uparrow	Num \uparrow	Time(s) \downarrow
U(PM) 2	89.02	42.22	3.60
w/o pyramid	76.94	37.94	3.02
w/o LoJoGM	14.21	12.93	3.33
w/o LoJoGM & pyramid	9.56	10.44	2.16

Extended Data Table 4. **Ablation study on the SceneFlow dataset.**

LoJoGM. LoJoGM achieves fine matches by leveraging local features based on multiple correlations. For the ablation of this module, we replace the LoJoGM module with a greedy optimization algorithm. Specifically, each source polygon selects the target polygon with the highest geometric similarity. Although this may not always lead to a globally optimal solution, it is optimal for each local match. The final matching performance in Table 4, evaluated by the ACR metric, decreases by approximately 80% compared to U(PM) 2 . This demonstrates that relying solely on the geometric features of polygons is inadequate for polygon matching, as these features are not robust to changes in viewpoint and segmentation variations.

5. Conclusion

A novel low-cost unsupervised polygon matching framework U(PM) 2 is proposed by integrating automatically learned features from pre-trained models with handcrafted features. 1) To our best knowledge, this work represents the first successful and effective attempt at direct polygon matching for stereo images, extending the feature matching paradigm to a higher semantic level without any training. 2) We addressed the challenges of scale variation in large-format images through bidirectional pyramid matching, significantly improving efficiency and expandability. 3) LoJoGM is proposed which mitigates the effect of local disparity discontinuities, enhancing the overall consistency of the matching results. 4) U(PM) 2 achieved SOTA accuracy with the satisfied speed on benchmarks in the polygon matching

task, with an average matching accuracy of 87%. Future research will target complex scenarios like dynamic occlusions.

References

- [1] Daniel Barath, Jana Noskova, Maksym Ivashechkin, and Jiri Matas. MAGSAC++, a fast, reliable and accurate robust estimator. In *2020 IEEE/CVF Conference on Computer Vision and Pattern Recognition (CVPR)*, pages 1301–1309, Seattle, WA, USA, 2020. IEEE. 4
- [2] Angela Dai, Angel X. Chang, Manolis Savva, Maciej Halber, Thomas Funkhouser, and Matthias Nießner. Scannet: Richly-annotated 3d reconstructions of indoor scenes. In *Proc. Computer Vision and Pattern Recognition (CVPR)*, IEEE, 2017. 6
- [3] Daniel DeTone, Tomasz Malisiewicz, and Andrew Rabinovich. SuperPoint: Self-supervised interest point detection and description. In *Proceedings of the IEEE Conference on Computer Vision and Pattern Recognition Workshops*, pages 224–236, 2018. 1
- [4] Abd Errahmane Kiouche, Hamida Seba, and Karima Amrouche. A maximum diversity-based path sparsification for geometric graph matching. *Pattern Recognition Letters*, 152: 107–114, 2021. 3, 5
- [5] Alexander Kirillov, Eric Mintun, Nikhila Ravi, Hanzi Mao, Chloe Rolland, Laura Gustafson, Tete Xiao, Spencer Whitehead, Alexander C. Berg, Wan-Yen Lo, Piotr Dollár, and Ross Girshick. Segment Anything, 2023. 1
- [6] Jinxiang Lai, Wenlong Wu, Bin-Bin Gao, Jun Liu, Jiawei Zhan, Congchong Nie, Yi Zeng, and Chengjie Wang. Matchdet: A collaborative framework for image matching and object detection. *Proceedings of the AAAI Conference on Artificial Intelligence*, 38(3):2858–2865, 2024. 3
- [7] Siyuan Li, Lei Ke, Martin Danelljan, Luigi Piccinelli, Mattia Segu, Luc Van Gool, and Fisher Yu. Matching anything by segmenting anything. In *Proceedings of the IEEE/CVF Conference on Computer Vision and Pattern Recognition*, pages 18963–18973, 2024. 1, 3
- [8] Xinyu Lin, Yingjie Zhou, Yipeng Liu, and Ce Zhu. A comprehensive review of image line segment detection and description: Taxonomies, comparisons, and challenges. *IEEE Transactions on Pattern Analysis and Machine Intelligence*, 46(12):8074–8093, 2024. 1
- [9] D.G. Lowe. Object recognition from local scale-invariant features. In *Proceedings of the Seventh IEEE International Conference on Computer Vision*, pages 1150–1157 vol.2, Kerkyra, Greece, 1999. IEEE. 1
- [10] Jianwen Luo and Elisa E. Konofagou. A fast normalized cross-correlation calculation method for motion estimation. *IEEE Transactions on Ultrasonics, Ferroelectrics, and Frequency Control*, 57(6):1347–1357, 2010. 3
- [11] N. Mayer, E. Ilg, P. Häusser, P. Fischer, D. Cremers, A. Dosovitskiy, and T. Brox. A large dataset to train convolutional networks for disparity, optical flow, and scene flow estimation. In *IEEE International Conference on Computer Vision and Pattern Recognition (CVPR)*, 2016. arXiv:1512.02134. 6

- [12] Moritz Menze, Christian Heipke, and Andreas Geiger. Object scene flow. *ISPRS Journal of Photogrammetry and Remote Sensing (JPRS)*, 2018. 6
- [13] Rémi Pautrat, Iago Suárez, Yifan Yu, Marc Pollefeys, and Viktor Larsson. GlueStick: Robust image matching by sticking points and lines together. In *Proceedings of the IEEE/CVF International Conference on Computer Vision*, pages 9706–9716, 2023. 1
- [14] Franz Rottensteiner. Isprs test project on urban classification and 3D building reconstruction: Evaluation of building reconstruction results. *Technical report*, 2013. 6, 7
- [15] Jiaming Sun, Zehong Shen, Yuang Wang, Hujun Bao, and Xiaowei Zhou. LoFTR: Detector-free local feature matching with transformers. In *2021 IEEE/CVF Conference on Computer Vision and Pattern Recognition (CVPR)*, pages 8918–8927, Nashville, TN, USA, 2021. IEEE. 1
- [16] Jintao Zhang, Zimin Xia, Mingyue Dong, Shuhan Shen, Linwei Yue, and Xianwei Zheng. Comatcher: Multi-view collaborative feature matching. In *Proceedings of the IEEE/CVF Conference on Computer Vision and Pattern Recognition (CVPR)*, pages 21970–21980, 2025. 3
- [17] Shihua Zhang, Zhenjie Zhu, Zizhuo Li, Tao Lu, and Jiayi Ma. Matching while perceiving: Enhance image feature matching with applicable semantic amalgamation. *Proceedings of the AAAI Conference on Artificial Intelligence*, 39(10):10094–10102, 2025. 1
- [18] Yeshe Zhang and Xu Zhao. MESA: Matching everything by segmenting anything. In *2024 IEEE/CVF Conference on Computer Vision and Pattern Recognition (CVPR)*, pages 20217–20226, Seattle, WA, USA, 2024. IEEE. 1, 3
- [19] Yeshe Zhang, Xu Zhao, and Dahong Qian. Searching from area to point: A hierarchical framework for semantic-geometric combined feature matching, 2024. 3

Appendix

Chang Li[†] Xingtao Peng

Key Laboratory for Geographical Process Analysis & Simulation of Hubei Province
Central China Normal University

lcschaka@126.com

lichang@ccnu.edu.cn

pengxt@mails.ccnu.edu.cn

1. Introduction

In this appendix, we provide comprehensive supplementary materials to support and extend the main content of the paper. The appendix is structured as follows:

- **2 Related Work:** We provide additional discussion on the pretrained models utilized in our framework.
- **3 Methodology:** This section elaborates on the mathematical formulations, detailed pseudocode and evaluation metrics involved in our work, including the formal definitions of the polygon matching, the equations used for template matching, polygon matching, and ground truth generation for polygon matching. Then, we provide detailed pseudocode for both the Bidirectional-Pyramid Matching and LoJoGM algorithms, offering a clear procedural overview of their implementation. Lastly, we describe the evaluation metrics used in our experiments, including ACR, SAS, and MP, along with justifications for their use. These derivations provide deeper insight into the mechanisms behind each stage and correspond to the *Bidirectional-Pyramid Matching*, *Local Matcher*, and *Metric for Polygon Matching* sections.
- **4 Experiments:** We detail the hardware and software environments used to run our experiments, as well as the hyperparameters employed for our method and baseline models. We include more extensive qualitative and quantitative results to validate the effectiveness of our method further. We provide in-depth discussion of the results in large-scale or challenging imagery. This corresponds to the *Experiments* section in the main paper.

We hope these supplementary materials offer valuable insights and facilitate reproducibility and a deeper understanding of our work.

2. Related work

Pre-trained model. A key advantage of using pre-trained models lies in their ability to enable low-cost training while

significantly reducing computational overhead. Pre-trained on large-scale datasets, these models [2, 3, 7, 9] acquire robust feature representation capabilities and can rapidly adapt to new tasks. This makes pre-trained models an efficient and low-cost solution for practical tasks. In this study, the SAM [3] is employed to segment polygons in images, providing initial matching sources. Point-based deep learning models such as LoFTR [8], SuperPoint [1], and Lightglue [5] are integrated as components for polygon matching.

Although polygon matching is fundamentally different from point matching task, polygons are essentially composed of points, so these pre-trained models are still applicable. Furthermore, we propose a paradigm of uniting automatically learned and handcrafted features, which utilizes high-level feature representations obtained from pre-trained models combined with textural and geometric (i.e., graphic) features of polygons to achieve generalizability in polygon matching task.

3. Methodology

3.1. Mathematical Formulation

3.1.1 Polygon matching

Let $\mathcal{A} = \{G_i\}_{i=1}^m$ denote the set of source polygons and $\mathcal{B} = \{G'_j\}_{j=1}^n$ denote the set of target polygons. Each polygon G_i (or G'_j) is represented by its set of geometric attributes and features.

We aim to find an optimal matching between polygons in \mathcal{A} and \mathcal{B} , subject to geometric constraints and features. The matching result is represented by a set of binary relation matrices:

$$M_{\text{adj}} \in \{0, 1\}^{m \times n} \quad (1)$$

where M_{adj} is a binary matrix indicating a valid matching configuration between \mathcal{A} and \mathcal{B} . Specifically, $M_{\text{adj}}(i, j) = 1$ if polygon $G_i \in \mathcal{A}$ is matched with polygon $G'_j \in \mathcal{B}$ in the n -th matching configuration, and $M_{\text{adj}}(i, j) = 0$ otherwise.

The goal is to determine the optimal relation E^* from

[†]Corresponding authors: Chang Li

this set that minimizes the global matching cost:

$$E^* = \arg \min_{M_{\text{adj}}} \sum_{i=1}^m \sum_{j=1}^n M'_{\text{adj}}(i, j) \cdot \text{Cost}(G_i, G'_j), \quad (2)$$

where $\text{Cost}(G_i, G'_j)$ measures the dissimilarity between two polygons based on shape and descriptors (i.e., features).

3.1.2 Template matching

In the sections *Bidirectional-pyramid matching* and *Texture similarity correlation*, we use normalized correlation coefficient templates to match similar texture features, ultimately obtaining the initial corresponding region or texture similarity R :

$$R(x, y) = \frac{\sum_{x'=0}^{w-1} \sum_{y'=0}^{h-1} (\mathbb{M}(T(x', y')) \cdot \mathbb{M}(I(x + x', y + y')))}{\sqrt{\sum_{x'=0}^{w-1} \sum_{y'=0}^{h-1} \mathbb{M}(T(x', y'))^2 \cdot \sum_{x'=0}^{h-1} \sum_{y'=0}^{h-1} \mathbb{M}(I(x + x', y + y'))^2}} \quad (3)$$

where $\mathbb{M}(\cdot)$ denotes mean centering, I and T are the image patch and target patch respectively. w and h are respectively the width and height of the image.

3.1.3 Ground truth generation of polygon matches

To identify the corresponding ground truth (GT) polygon for a given polygon G_i from another image, we employ a multi-faceted similarity analysis. The core of this process is to quantify the relationship between a polygon from a source image, G_L , and all candidate polygons in a target image, $\{G_R\}$. This is achieved by first projecting G_L into the coordinate system of the target image via a transformation T , yielding $G'_L = T(G_L)$. Subsequently, a comprehensive similarity score is calculated.

The similarity between the projected source polygon G_i and a target polygon G_j is defined by a weighted aggregation of five distinct metrics. Each metric evaluates a specific aspect of their relationship, from geometric congruity to spatial proximity. The comprehensive similarity score $S(G_i, G_j)$ is formulated as:

$$S(G_i, G_j) = \alpha \cdot \text{IoU}(G'_i, G_j) + \beta \cdot H^{\text{inv}}(G'_i, G_j) + \kappa \cdot C^{\text{inv}}(G'_i, G_j) + \delta \cdot R(G'_i, G_j) + D(G'_i, G_j) \quad (4)$$

$(\cdot)^{\text{inv}}$ denotes the unified transformation of the original function, designed to increase when the original function decreases, and vice versa. The contribution of each metric to the final score is controlled by a set of weights: $\alpha, \beta, \kappa, \delta$. In the quantitative experiment in the main text, we used three different thresholds $\alpha \in \{40\%, 50\%, 80\%\}$ to generate different GT values for evaluating the experiment, in order to

reduce the experimental error caused by the deviation of GT values. The components of this formula are detailed below:

Intersection over Union (IoU) measures the overlap between the two polygons:

$$\text{IoU}(G_1, G_2) = \frac{\text{Area}(G_1 \cap G_2)}{\text{Area}(G_1 \cup G_2)} \quad (5)$$

Inverse Hausdorff Distance (H^{inv}) measures the similarity based on the maximum distance between the contours of the two polygons. We use its inverse to ensure higher values indicate greater similarity:

$$H^{\text{inv}}(G_1, G_2) = \frac{1}{1 + H(G_1, G_2)} \quad (6)$$

$$H(G_1, G_2) = \max \left(\max_{p \in G_1} \min_{q \in G_2} d(p, q), \max_{q \in G_2} \min_{p \in G_1} d(p, q) \right) \quad (7)$$

$d(p, q)$ denotes the distance between node p and node q .

Inverse Chamfer Distance (C^{-1}) The Inverse Chamfer Distance provides a stable measure of similarity by averaging the distances between the vertices of the two polygons. The Chamfer distance $C(G_1, G_2)$ is computed by first finding the mean distance from vertices in one polygon to their nearest neighbors in the other, and then averaging this value for both directions. The formula is:

$$C(G_1, G_2) = \frac{1}{2} \left(\frac{1}{|G_1|} \sum_{p \in G_1} \min_{q \in G_2} d(p, q) + \frac{1}{|G_2|} \sum_{q \in G_2} \min_{p \in G_1} d(p, q) \right) \quad (8)$$

This value is then transformed into a similarity metric, where higher values indicate a better match:

$$C^{\text{inv}}(G_1, G_2) = \frac{1}{1 + C(G_1, G_2)} \quad (9)$$

In addition to shape, we consider relative size and location.

Area Ratio Similarity (R) compares the relative sizes of the original polygons to penalize significant scale differences:

$$R(G_i, G_j) = \frac{\min(\text{Area}(G_i), \text{Area}(G_j))}{\max(\text{Area}(G_i), \text{Area}(G_j))} \quad (10)$$

Distance Penalty (D) applies a penalty based on the Euclidean distance between the centroids of the projected and target polygons. The penalty is modeled as a negative Gaussian function, which becomes more severe as the distance increases:

$$D(G'_i, G_j) = \exp \left(-\frac{d^2(\text{center}(G'_i), \text{center}(G_j))}{2\sigma^2} \right) - 1 \quad (11)$$

where the parameter σ is set to 40.

For a given polygon G_i , we compute its similarity score with all candidate polygons in the target image. The candidate with the highest score, denoted G_{j^*} , is considered the best potential match. However, to confirm this match, two conditions must be satisfied.

Absolute Similarity: The similarity score of the best match must exceed a minimum threshold.

$$S(G_i, G_{j^*}) > \text{threshold} \quad (12)$$

Match Uniqueness: The match must be unambiguous. We quantify this using a confidence score, which measures the margin between the best and the second-best match. This confidence must be above a certain level λ .

$$\text{confidence} = S(G_i, G_{j^*}) - \max_{j \neq j^*} S(G_i, G_j) > \lambda \quad (13)$$

Therefore, a polygon G_j is confirmed as the corresponding ground truth polygon for G_i if and only if it is the highest-scoring candidate and both the absolute similarity and confidence criteria are met. This dual-condition approach ensures that the identified matches are both strong and unique.

3.2. Algorithm Pseudocode

3.2.1 Bidirectional-Pyramid Matching

The initial coarse matching between polygons is established through a hierarchical search process detailed in Algorithm 1. This process operates on Gaussian image pyramids to efficiently handle large images. The matching begins at the top, lowest-resolution level of the pyramid and iteratively refines the search area down to the original image resolution. At each level, a template from the source image is matched within a search window in the target image to find the most correlated region. This search is constrained by epipolar geometry to filter out geometrically implausible matches. The resulting matched region from a higher level is then projected down to define a more constrained search window for the next, finer level.

This iterative refinement continues through the pyramid layers, progressively narrowing the search area. The outcome for each source polygon is a small, final search window (W_{final}) in the target image. Any target polygons located within this final window are considered candidate matches, resulting in a many-to-many coarse matching matrix. This matrix serves as the input for a subsequent refinement stage, which aims to resolve ambiguities and establish a one-to-one mapping.

3.2.2 Hungarian Polygon Matching

To resolve the ambiguous, many-to-many relationships produced by the initial coarse matching, we introduce Hungarian Polygon Matching in the Local-joint Geometry and

Algorithm 1 Bidirectional-pyramid matching

```

1: Construct search window  $W_\phi$  with  $c_i$  and  $\phi$ 
2: Crop template  $A$  from layer  $k$  of image  $X$  using window
    $W_\phi$ 
3: if  $k == 0$  then
4:   Set  $\tau \leftarrow 25$ 
5:   Construct search window  $W_\tau$  with center  $c'_i$  and size
    $\tau$ 
6: else
7:   Map final search window  $W_\phi$  from layer  $k - 1$  to
   current layer as  $W_\tau$ 
8: end if
9: Crop search area  $S$  from layer  $K$  of image  $Y$  using
   window  $W_\tau$ 
10: Perform template matching between  $A$  and  $S$  to find
   most correlated point  $c''$ 
11: Construct new search window  $W_\phi$  centered at  $c''$  with
   size  $\phi$ 

```

Multi-feature Matching (LoJoGM) strategy, detailed in Algorithm 2. This approach pioneers the use of the Hungarian algorithm to establish a globally optimal set of one-to-one polygon matches within a local neighborhood. The process begins by constructing a cost matrix where each entry represents the cost of matching a pair of polygons, calculated as the inverse of their comprehensive similarity score. Subsequently, the Hungarian algorithm is applied to this matrix to solve the assignment problem. This identifies the unique pairing of polygons that minimizes the total matching cost across the entire set, effectively resolving local topological inconsistencies and disparity mutations by finding the most coherent overall solution, rather than relying on isolated greedy choices. The final output is a refined adjacency matrix representing the optimal, unambiguous matches.

4. Experiments

4.1. Evaluation Metrics

4.1.1 Area Coverage Ratio

To provide a more accurate and meaningful evaluation of matching performance, we propose the Area Coverage Ratio (ACR). This metric is designed as a refinement of the Area of Overlap Ratio (AOR) found in benchmarks like MESA [11]. A primary limitation of AOR is that it measures the matched area against the total image area, which can produce misleadingly high scores for methods that result in significant over-coverage. An algorithm could incorrectly match large, irrelevant regions and still be rewarded.

The ACR addresses this flaw by focusing the evaluation specifically on the objects of interest. It is calculated not against the entire image, but as the ratio of the total area of

Algorithm 2 Hungarian Polygon Matching

Require: Polygon list A , Polygon list B , Match threshold ι , Helper parameters θ

Ensure: Match matrix M_{adj}

- 1: Initialize matrix C of size $|A| \times |B|$ with a large value
- 2: Initialize matrix M_{adj} of size $|A| \times |B|$ with zeros
- 3: **for** $i \leftarrow 0$ to $|A| - 1$ **do**
- 4: $a \leftarrow A[i]$
- 5: **for** $j \leftarrow 0$ to $|B| - 1$ **do**
- 6: $b \leftarrow B[j]$
- 7: **if** a and b have a reciprocal relationship **then**
- 8: $\text{similarity} \leftarrow \text{calculate_similarity}(a, b, \theta)$
- 9: $C[i, j] \leftarrow 1/(\text{similarity} + \epsilon)$ {Cost is inverse of similarity}
- 10: **end if**
- 11: **end for**
- 12: **end for**
- 13: **for** each pair of indices (i, j) in $\text{zip}(\text{row}, \text{col})$ **do**
- 14: **if** $C[i, j] < \iota$ **then**
- 15: $M_{\text{adj}}[i, j] \leftarrow 1$
- 16: **end if**
- 17: **end for**
- 18: **return** M_{adj}

correctly matched polygons to the total area of all ground truth polygons available for matching. This ensures the metric directly reflects the algorithm’s capability to identify semantically significant regions, providing a more robust and intuitive measure of performance that penalizes both missed polygons and irrelevant matches. The formula is given by:

$$\text{ACR} = \frac{\sum \text{Area}(\text{matched})}{\sum \text{Area}(\text{GT})} \quad (14)$$

4.1.2 Matching Precision

To quantitatively evaluate the geometric precision of our matching results, we define the Matching Precision (MP). This metric is designed to be robust to topological inconsistencies in segmentation by comparing the total matched area.

Let the sets of predicted matched polygons in the left and right images be P_L^{pred} and P_R^{pred} , and the corresponding ground truth sets be P_L^{gt} and P_R^{gt} . We first compute a single unified region for each set via $\mathcal{U}(P)$. The MP is then the mean of the IoU calculated as follows:

$$\text{MA} = \frac{1}{2} \left(\text{IoU}(\mathcal{U}(P_L^{\text{pred}}), \mathcal{U}(P_L^{\text{gt}})) + \text{IoU}(\mathcal{U}(P_R^{\text{pred}}), \mathcal{U}(P_R^{\text{gt}})) \right) \quad (15)$$

The primary advantage of MP is its robustness to segmentation differences. By aggregating all matched polygons

into a single region before computing IoU, the MA score correctly evaluates the total spatial overlap, making it insensitive to one-to-many or many-to-one correspondences. This ensures algorithms are rewarded for accurately identifying the overall matched region, rather than being penalized for minor differences in polygonization. Furthermore, its formulation provides an unbiased assessment, independent of which image is considered the source.

4.1.3 Symmetric Area Score

To effectively evaluate matching performance, particularly in scenarios prone to over-coverage, we introduce the Symmetric Area Score (SAS). Traditional metrics often fail to penalize results where the matched area is excessively large compared to the ground truth, which does not reflect real-world performance requirements where both over-matching and under-matching are undesirable. The SAS is designed to address this by symmetrically penalizing any deviation from the ideal coverage ratio.

The score is based on the ratio of the total area of predicted matched polygons to the total area of the ground truth polygons. The core of the SAS lies in its formulation, which ensures that a ratio greater than one (over-coverage) is penalized to the same degree as a ratio less than one (under-coverage). A perfect area match yields a score of 1, which decays exponentially as the ratio deviates from this ideal. This provides a balanced and realistic assessment of how well the predicted area corresponds to the ground truth. In our implementation, the score is calculated as:

$$\text{SAS} = \exp(-z \cdot |\ln(\text{ACR})|) \quad (16)$$

z is scaling factor, used to control penalties.

4.2 Experimental Settings

All experiments were conducted using an i7-14700K CPU and two L40 (48GB) GPUs. We summarize the key hyperparameters used in our experiments as follows, and all hyperparameters used in our method are empirically determined based on test. All images are kept at their original resolutions: 1296×968 for ScanNet, 960×540 for Scene-Flow, and 1242×375 for KITTI.

In Algorithm 1, the local window size τ is set to 25. In Algorithm 2, the similarity threshold ι is set to 5. For Sec. Ground Truth Generation of Polygon Matches, the absolute similarity threshold is fixed at 0.3. α is $(0.8, 0.5, 0.4)$, β and κ are $1/8(1 - \alpha)$, and δ is $3/4(1 - \alpha)$. The value of γ in the main text Eq. (8) is 8. The geometric similarity weights are 5, 6, and 7 (Table 1 in this appendix and Table 5 in the main text). The confidence level λ is 0.1. Scaling factor z is 5.

4.3. Quantitative experiment

4.3.1 Evaluations on other datasets

We conduct additional experiments on the SceneFlow and KITTI datasets to evaluate the sensitivity of $U(PM)^2$ under different geometric similarity weights (5/6/7), while keeping all other hyperparameters fixed. As shown in Table 1, variations in geometric similarity weights result in only minor performance differences within each experiment group, with the maximum ACR deviation not exceeding 0.52. This indicates that $U(PM)^2$, by leveraging LoJoGM to integrate geometric and texture similarities under a globally optimal matching scheme, exhibits strong robustness to both dataset complexity (e.g., KITTI) and hyperparameter variations.

Dataset	Method	ACR↑	Num↑	Time↓
SceneFlow	$U(PM)^2$ @5	89.19	43.22	9.95
	$U(PM)^2$ @6	89.34	43.27	9.95
	$U(PM)^2$ @7	89.53	43.33	9.93
KITTI	$U(PM)^2$ @5	80.78	29.49	7.78
	$U(PM)^2$ @6	81.26	29.55	7.77
	$U(PM)^2$ @7	81.50	29.60	7.79

Extended Data Table 1. **Evaluation on SceneFlow and KITTI datasets for conventional metrics.** $U(PM)^2$ was evaluated under different weights (@5/@6/@7) between the area discrepancy and shape differences in geometric correlation.

4.3.2 Matching in challenging imagery

To validate the scalability and efficiency of our proposed $U(PM)^2$ framework in challenging imagery, we conducted experiments on large-format stereo-image pairs (Table 3 in the main text). ISPRS remote dataset [6] presents significant challenges due to its high resolution between images. Specifically, we assessed the impact of our bidirectional pyramid matching strategy on both matching accuracy and computational efficiency. By varying the number \mathcal{L} of pyramid levels, we aimed to demonstrate the trade-off between speed and performance. Taking into account the efficiency, we use SIFT operators instead of LoFTR in the large format matching task, they are faster and extract more feature points in that scenario. We hypothesized that the pyramid approach would significantly reduce matching time while maintaining acceptable accuracy, particularly in comparison to a baseline approach that operates directly on full-resolution images. Furthermore, we measured the matching time to assess the computational efficiency of our method. Table 3 presents the quantitative results of our experiments, showcasing the effectiveness of $U(PM)^2$ in handling large-format images.

4.3.3 The impact of SAM on segmentation quality

We have evaluated the influence of SAM [3] with different parameter sizes on the matching quality. Preliminary results are shown in Table 2. SAM with the largest parameters acquired the highest performance.

Model	Recall(%)	Precision(%)	F1
vit-h	72.72	87.15	0.79
vit-l	57.11	78.40	0.66
vit-b	59.67	82.60	0.69

Extended Data Table 2. Impact of SAM segmentation quality with different parameter sizes on $U(PM)^2$ matching performance.

4.4. Qualitative experiment

We present qualitative results on the SceneFlow and ScanNet datasets in Figure 1 and Figure 2, respectively. Compared to other methods, our method performs better in capturing fine details and structures. More importantly, our $U(PM)^2$ can correspond to each nonsemantic patch in stereo image pairs. $U(PM)^2$ exhibits consistent performance across different combinations of feature detectors and matchers, as both settings successfully align corresponding polygons in the images. This robustness stems from its core components (i.e., the bidirectional pyramid matching strategy and LoJoGM) which effectively handle disparity discontinuities and enforce globally optimal matching. These capabilities are beyond the scope of conventional point-based matchers.

In contrast, competing methods such as MESA [11] and SGAM [10] suffer from significant matching redundancy, resulting in highly overlapping matched regions. This overlap introduces ambiguity in polygon matching. MASA [4] suffers from insufficient matching because of training requirements. To address this challenge, $U(PM)^2$ introduces a dedicated local matcher, specifically designed to suppress redundant matches and ensure precise correspondence without any training.

References

- [1] Daniel DeTone, Tomasz Malisiewicz, and Andrew Rabinovich. SuperPoint: Self-supervised interest point detection and description. In *Proceedings of the IEEE Conference on Computer Vision and Pattern Recognition Workshops*, pages 224–236, 2018. [1](#)
- [2] Hanwen Jiang, Arjun Karpur, Bingyi Cao, Qixing Huang, and André Araujo. OmniGlue: Generalizable feature matching with foundation model guidance. In *Proceedings of the IEEE/CVF Conference on Computer Vision and Pattern Recognition*, pages 19865–19875, 2024. [1](#)
- [3] Alexander Kirillov, Eric Mintun, Nikhila Ravi, Hanzi Mao, Chloe Rolland, Laura Gustafson, Tete Xiao, Spencer Whitehead, Alexander C. Berg, Wan-Yen Lo, Piotr Dollár, and Ross Girshick. Segment Anything, 2023. [1, 5](#)

[4] Siyuan Li, Lei Ke, Martin Danelljan, Luigi Piccinelli, Mattia Segu, Luc Van Gool, and Fisher Yu. Matching anything by segmenting anything. In *Proceedings of the IEEE/CVF Conference on Computer Vision and Pattern Recognition*, pages 18963–18973, 2024. 5

[5] Philipp Lindenberger, Paul-Edouard Sarlin, and Marc Pollefeys. LightGlue: Local feature matching at light speed. In *Proceedings of the IEEE/CVF International Conference on Computer Vision*, pages 17627–17638, 2023. 1

[6] Franz Rottensteiner. Isprs test project on urban classification and 3D building reconstruction: Evaluation of building reconstruction results. *Technical report*, 2013. 5

[7] Xuelun Shen, Zhipeng Cai, Wei Yin, Matthias Müller, Zijun Li, Kaixuan Wang, Xiaozhi Chen, and Cheng Wang. GIM: Learning generalizable image matcher from internet videos, 2024. 1

[8] Jiaming Sun, Zehong Shen, Yuang Wang, Hujun Bao, and Xiaowei Zhou. LoFTR: Detector-free local feature matching with transformers. In *2021 IEEE/CVF Conference on Computer Vision and Pattern Recognition (CVPR)*, pages 8918–8927, Nashville, TN, USA, 2021. IEEE. 1

[9] Yunyang Xiong, Bala Varadarajan, Lemeng Wu, Xiaoyou Xiang, Fanyi Xiao, Chenchen Zhu, Xiaoliang Dai, Dilin Wang, Fei Sun, Forrest Iandola, Raghuraman Krish

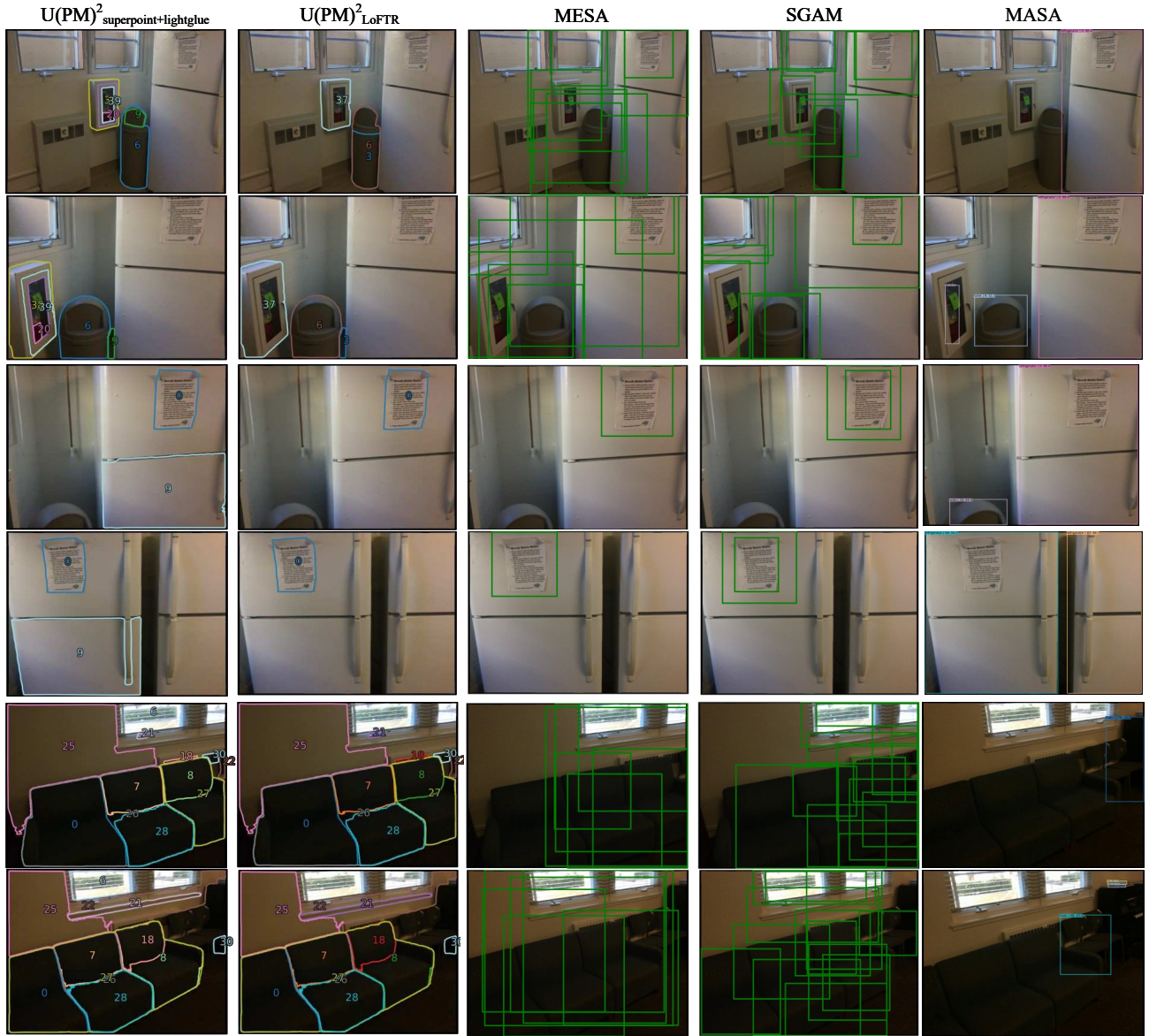


Figure 1. Qualitative results on the ScanNet dataset. In the same column of images, the images in the upper and lower rows that are adjacent to each other form a pair of stereo images.

namoorthi, and Vikas Chandra. EfficientSAM: Leveraged Masked Image Pretraining for Efficient Segment Anything. <https://arxiv.org/abs/2312.00863v1>, 2023. 1

[10] Yesheng Zhang and Xu Zhao. DMESA: Densely matching everything by segmenting anything, 2024. 5

[11] Yesheng Zhang and Xu Zhao. MESA: Matching everything by segmenting anything. In *2024 IEEE/CVF Conference on Computer Vision and Pattern Recognition (CVPR)*, pages 20217–20226, Seattle, WA, USA, 2024. IEEE. 3, 5



Figure 2. Qualitative results on the SceneFlow dataset. In the same column of images, the images in the upper and lower rows that are adjacent to each other form a pair of stereo images.